THE JOURNAL OF BIOLOGICAL CHEMISTRY
Vol. 278, No. 51, Issue of December 19, pp. 51015–51022, 2003

Printed in U.S.A.

Two Conformations of Archaeal Ssh10b

THE ORIGIN OF ITS TEMPERATURE-DEPENDENT INTERACTION WITH DNA*

Received for publication, August 4, 2003, and in revised form, September 29, 2003
Published, JBC Papers in Press, September 30, 2003, DOI 10.1074/jbc.M308510200

Qiu Cui‡§, Yufeng Tong‡§, Hong Xue¶, Li Huang¶, Yingang Feng‡, and Jinfeng Wang‡‖

From the ‡National Laboratory of Biomacromolecules, Center for Molecular Biology, Institute of Biophysics, Chinese Academy of Sciences, 15 Datun Road, 100101 Beijing, China and ¶State Key Laboratory of Microbial Resources, Institute of Microbiology, Chinese Academy of Sciences, 100080 Beijing, China

The DNA-binding protein Ssh10b from the hyperthermophilic archaeon *Sulfolobus shibatae* is a member of the Sac10b family, which has been speculated to be involved in the organization of the chromosomal DNA in Archaea. Ssh10b affects the DNA topology in a temperature dependent fashion that has not been reported for any other DNA-binding proteins. Heteronuclear NMR and site-directed mutagenesis were used to analyze the structural basis of the temperature-dependent Ssh10b-DNA interaction. The data analysis indicates that two forms of Ssh10b homodimers co-exist in solution, and the slow *cis-trans* isomerization of the Leu^{61}-Pro^{62} peptide bond is the key factor responsible for the conformational heterogeneity of the Ssh10b homodimer. The T-form dimer, with the Leu^{61}-Pro^{62} bond in the *trans* conformation, dominates at higher temperature, whereas population of the C-form dimer, with the bond in the *cis* conformation, increases on decreasing the temperature. The two forms of the Ssh10b dimer show the same DNA binding site but have different conformational features that are responsible for the temperature-dependent nature of the Ssh10b-DNA interaction.

Proteins of the Sac10b family are highly conserved among thermophilic and hyperthermophilic Archaea, and homologous sequences have also been identified in eukaryal proteins from higher plants, protists, and vertebrates (1–3). The members of this family have been postulated to play a role in chromosomal organization in Archaea since the initial isolation of Sac10b from the hyperthermophile *Sulfolobus acidocaldarius* in the mid-1980s. Sac10b exists as a dimer of two 10-kDa subunits in solution and binds to DNA nonspecifically (4, 5). Electron microscopic studies have shown that Sac10b binds to DNA cooperatively and forms different protein-DNA complexes depending on protein/DNA ratios but does not induce DNA supercoiling or compact DNA (6).

Recently, Bell *et al.* (2) discovered that Alba (also named Sso10b, a member of Sac10b family) forms a specific complex with a Sir2 homolog in *Sulfolobus solfataricus* cell extracts. They found that Sir2 in the presence of NAD^+ can regulate the DNA binding affinity of Alba by deacetylation of Lys^{16} of the protein. More recently, the crystal structure of Alba has been solved. Interestingly, the protein shares structural homology to the C-terminal domain of the *Escherichia coli* translation factor IF3 and the N-terminal DNA binding domain of DNase I. A model for the Alba-DNA interaction has been proposed (7).

Ssh10b, another member of the Sac10b family, was isolated from *Sulfolobus shibatae* (1). The protein is highly abundant and basic and binds double-stranded DNA without apparent sequence specificity. Gel retardation assays have shown that Ssh10b has two modes of DNA binding with distinctively different binding densities. In the low binding density mode, Ssh10b exhibits a binding size of ~12 bp of DNA, whereas in the high binding density mode, the protein appears to bind shorter stretches of DNA. Interestingly, Ssh10b affects DNA topology in a temperature-dependent fashion; it is capable of significantly constraining DNA in negative supercoils at temperatures higher than 318 K, but this ability is drastically reduced at 298 K (1). A previous NMR study revealed the co-existence of two forms of Ssh10b dimers at temperatures between 283 and 320 K, with one dominating at lower temperatures and the other at higher temperatures (8). However, the structural basis for the conformational heterogeneity of the Ssh10b dimer and the temperature dependence of the interaction of Ssh10b with DNA remained to be clarified.

In the present study, we investigated the heterogeneous conformations of Ssh10b and the structural factors influencing the interaction of Ssh10b with DNA by heteronuclear NMR spectroscopy. We found that the *cis-trans* isomerization of the Leu^{61}-Pro^{62} peptide bond of Ssh10b is the primary determinant of the conformational heterogeneity of the Ssh10b dimer. We also found that the equilibrium between the *cis-* and *trans-*forms of Ssh10b is sensitive to temperature. Our data suggest that the effect of temperature on the capacity of the protein to constrain negative DNA supercoils is related to the temperature-dependent conversion between the two Ssh10b conformations.

EXPERIMENTAL PROCEDURES

Expression and Purification of Ssh10b and Its Mutants—Ssh10b was produced from a synthetic gene with codon usage optimized for expression in *E. coli*. The gene was created from 12 overlapping oligonucleotides primers that were ligated and then cloned into the EcoRI and BamHI sites of vector pBV220. The genes of Δ8 (deletion of the N-terminal eight residues), Δ8P18A (Pro^{18} replaced by Ala of the Δ8 mutant), and P62A (Pro^{62} replaced by Ala) mutants of Ssh10b were obtained by primer-directed mutagenesis. Each gene was cloned into expression vector pET11c, and the products were used to transform *E. coli* BL21(DE3) cells. The transformed cultures were grown at 37 °C in 1 liter of LB broth containing 50 mg/liter ampicillin until A_{600} = 0.8–1.0, and expression was induced for 2 h by adding isopropyl-1-thio-β-D-galactopyranoside to a final concentration of 1 mM. The harvested cells were resuspended in 20 ml of buffer containing 30 mM potassium phosphate, pH 6.6, 0.1 mM EDTA, and 1 mM phenylmethylsulfonyl fluoride and sonicated. The lysate was centrifuged at 150,000 × *g* for 2.5 h at 4 °C and then the supernatant was heated for 20 min at 80 °C to precipitate the *E. coli* proteins. After centrifugation, the supernatant

* This work was supported in part by the National Natural Science Foundation of China Grants 39823001, 30270301, 39925001, and 30030010. The costs of publication of this article were defrayed in part by the payment of page charges. This article must therefore be hereby marked "*advertisement*" in accordance with 18 U.S.C. Section 1734 solely to indicate this fact.

§ Contributed equally to this work.

‖ To whom correspondence should be addressed. Tel.: 86-10-64888490; Fax: 86-10-64872026; E-mail: jfw@sun5.ibp.ac.cn.

was applied to a Resource-S column. Bound proteins were eluted with a 50-ml KCl gradient (0 to 0.75 M). Fractions containing Ssh10b proteins were pooled, dialyzed against distilled de-ionized water, and finally lyophilized. The purity of the proteins was confirmed by SDS-PAGE to be more than 95% and by matrix-assisted laser desorption ionization time-of-flight to be free of nucleic acid contaminants.

NMR Sample Preparation—^{15}N or ^{13}C singly labeled and $^{15}N/^{13}C$ doubly labeled Ssh10b proteins were expressed in *E. coli* strain BL21(DE3) grown in M9 minimal medium using $^{15}NH_4Cl$ and/or ^{13}C-glucose as the sole nitrogen and carbon sources. All protein samples for NMR measurements were dissolved in 500 μl of 90% H_2O/10% D_2O containing 20 mM deuterated acetate buffer, pH 4.8, 50 μl of NaN_3, 1 μM 2,2-dimethyl-2-silapentanesulfonic acid and 20 mM KCl to a final protein concentration of about 1 mM, unless otherwise indicated. The sample for determination of the dimer interface of Ssh10b was $^{15}N/^{13}C$ asymmetrically labeled.

NMR Spectroscopy—All NMR experiments were carried out on a Bruker DMX 600 spectrometer equipped with a triple resonance probe and an actively shielded three-axis gradient unit. The experimental temperature was set to 310 K except for the temperature-dependent experiments. ^1H chemical shifts were referenced to the internal standard 2,2-dimethyl-2-silapentanesulfonic acid at 0 ppm. ^{15}N and ^{13}C chemical shifts were calculated indirectly using the corresponding consensus Ξ ratios (9).

Although the assignment of the T-form Ssh10b has already been published (8), assignment of the remaining resolved resonances of the C-form Ssh10b was achieved by further exploring existing spectra: 3D ^1H-^{13}C-^{15}N HNCA, HN(CA)CO, CBCA(CO)NH, HNCACB, and HNCO experiments for backbone assignments and HBHA(CBCA)NH, HBHA(CBCACO)NH, and CC(CO)NH, as well as 3D ^1H-^{13}C HCCH-TOCSY experiments for side chain assignments. Most of the backbone assignments of [P62A]Ssh10b was obtained by comparison with Ssh10b; the remaining ambiguities were resolved with an HNCA experiment. A 3D NOESY-^1H,^{13}C-HMQC experiment was carried out to distinguish the *cis* and *trans* conformations of the X-prolyl bond of Ssh10b. Conformational exchange of Ssh10b was monitored using a series of 2D ^1H-^{15}N correlation experiments for simultaneous measurements of ^{15}N longitudinal decay and chemical exchange rates at exchange delays of 12, 52, 152, 302, 452, 552, 652, 902, 1102, 1302, and 1602 ms (10). The temperature dependence of 2D ^1H-^{15}N HSQC spectra of Ssh10b was measured at temperatures ranging from 283 to 330 K at increments of 3.5 K. To determine residues involved in the dimer interface, a 2D version of the four-dimensional ^1H,^{13}C-HMQC-^1H,^1H-NOESY-^1H,^{15}N-HSQC experiment (11) was carried out on the $^{15}N/^{13}C$ asymmetrically labeled Ssh10b sample, and ^{15}N was allowed to evolve in the indirect dimension. The mixing time of the experiment was 150 ms. 2D intensity modulated HSQC (12) was used to measure the $^3J_{NH\alpha}$ coupling constants on ^{15}N singly labeled proteins. The delay for ^3J coupling evolution was set to 30 ms. 2D ^1H-^{15}N HSQC experiments were also used for exploring the binding behavior of Ssh10b with synthesized 16-bp double-strand DNA fragments (5′-GGCAGACGCGTCTGCC).

All NMR data were processed and analyzed using Felix 98 (Accelrys Inc.). The data points in each indirect dimension were usually doubled by linear prediction and zero-filled. A 90 to 60° shifted square sine bell apodization was used for all dimensions prior to Fourier transformation.

Electrophoretic Mobility Shift Assay (EMSA)—A 108-bp double-stranded DNA fragment (5′-CGACGTTGTA AAACGACGGC CAGTGCCAAG CTTGGCTGCA GGTCGACGGA TCCCCCCAAT GCTTCGTTTC GTATCACACA CCCCAAAGCC TTCTGCTTTG AATGCTGCC) was labeled at the 5′-end with [γ-^{32}P]ATP. The labeled fragment was incubated with Ssh10b or [P62A]Ssh10b for 15 min at either 293 or 320 K. The reaction mixture of 20 μl contained 0.5 to 1 ng of DNA fragment, 0.01 to 2.5 μM Ssh10b or [P62a]Ssh10b, 20 mM Tris-HCl, 1 mM dithiothreitol, 100 μg/ml bovine serum albumin, pH 7.6. Protein-DNA complexes were loaded on 5% polyacrylamide gel in 0.1× Tris-Borate-EDTA (13) and run at a constant voltage. The temperature of the samples was maintained at either 293 or 320 K using a circulating water bath. Following electrophoresis, the gel was exposed to x-ray film.

Nick Closure Assay—The single-nick plasmid pUC18 was prepared as described previously (14). The nicked plasmid (1 μg) was incubated with Ssh10b or [P62A]Ssh10b at various mass ratios for 5 min at temperatures of 298 or 330 K. The ligating reactions were then performed as described previously (15). T4 DNA ligase (3 Weiss units) and Pfu DNA ligase (4 Weiss units) were used for the reactions carried out at 298 and 330 K, respectively. After the ligation reaction, the samples were analyzed by 1.4% agarose electrophoresis in 0.5× Tris-Phosphate-EDTA (13).

[1] The abbreviations used are: 3D, three-dimensional; 2D, two-dimensional; EMSA, electrophoretic mobility shift assay; NOE, nuclear Overhauser effect; dsDNA, double-stranded DNA.

RESULTS

Co-existence of Two Ssh10b Homodimers with Different Conformations—As shown in the previous study, two sets of cross-peaks (for simplicity denoted as "doublets" hereafter) are observed for most residues of Ssh10b in the 2D ^1H-^{15}N HSQC spectrum (Fig. 1*A*) (8). The signal intensities of the resonance doublets are not equal, with one signal stronger than the other in all doublets. Although the results of chemical cross-linking (1) and the related crystal structure (7) suggest that Ssh10b is a dimer, the resonance doublets with unequal signal intensities (Fig. 1*A*) cannot be attributed to an asymmetric arrangement of the two monomeric units of the Ssh10b molecule under the sample conditions used in the NMR experiments, as in this case the intensities of the two resonance signals in the doublet should be equal. The chemical shift differences between the higher (δ_H) and lower (δ_L) intensity resonance signals in the doublets in Fig. 1*A* were calculated as the weighted differences between the ^{15}N ($\Delta\delta_N = \delta_{N,H} - \delta_{N,L}$) and ^1H_N ($\Delta\delta_{HN} = \delta_{HN,H} - \delta_{HN,L}$) values, according to $\Delta\delta = (\Delta\delta_{HN}^2 + 0.17\Delta\delta_N^2)^{1/2}$ (Fig. 2) (16). Although both monomer and dimer crystal forms of Alba have been obtained (7), the $\Delta\delta$ values make it clear that the Ssh10b molecule does not exist as a mixture of dimeric and monomeric forms in solution. If this were the case, then the resonance doublets should be observed only for residues located at the dimer interface. The cross-peaks shown in Fig. 3 correspond to the residues at the Ssh10b dimer interface, detected by X-nucleus edited NOESY. When mapped to the sequence, the data indicate that helix α_2, a portion near the C-terminal of strand β_3, and the N-terminal part of strand β_4 are involved in the dimeric surface (Fig. 4*A*). However, $\Delta\delta$ values (Fig. 2) reveal that the residues of the N-terminal part of strand β_4 give only "singlet" signals, whereas residues in helix α_1 and strands β_1 and β_2, which are distant from the interface, generate doublet signals (Fig. 4*B*). The line widths for each pair of doublets are the same. In addition, the ratios of the signal intensities of the doublets are independent of the concentrations (0.05–1.5 mM) of Ssh10b as revealed by NMR experiments (data not shown). These therefore also exclude the possibility of an oligomerization equilibrium. Because Ssh10b is dimeric as confirmed by size-exclusion chromatography (data not shown), it was considered whether two forms of Ssh10b dimer might co-exist in solution. The form with higher signal intensity in doublets was assigned as the T-form and the other with lower signal intensity as the C-form. No "multiplets" other than doublets were observed for most residues of Ssh10b (Fig. 1*A*), consistent with both the T-form and the C-form as homodimers, with the monomeric subunits arranged symmetrically in each dimer.

The main-chain torsion angle ϕ is closely related to the backbone conformation of proteins and can be calculated from the $^3J_{NH\alpha}$ scalar coupling constants. The J-coupling constants of Ssh10b were measured by 2D intensity modulated HSQC (12). The differences between the $^3J_{NH\alpha}$ value for the T-form and for the C-form ($\Delta^3J_{NH\alpha}$) at each residue position is shown in Fig. 2. Residues with an absolute $\Delta^3J_{NH\alpha}$ value greater than 1 Hz are found in segments spanning the whole molecule: the N-terminal region, the loop linking strand β_1 and helix α_1, helices α_1 and α_2, and the C-terminal of strand β_4. This suggested that the main-chain conformations are different in the two forms of the Ssh10b dimer.

Cis and Trans Conformations of Ssh10—Fig. 5 shows portions of a ^1H-^{15}N heteronuclear chemical exchange spectrum at an exchange delay of 1.3 s (10). Two categories of doublets,

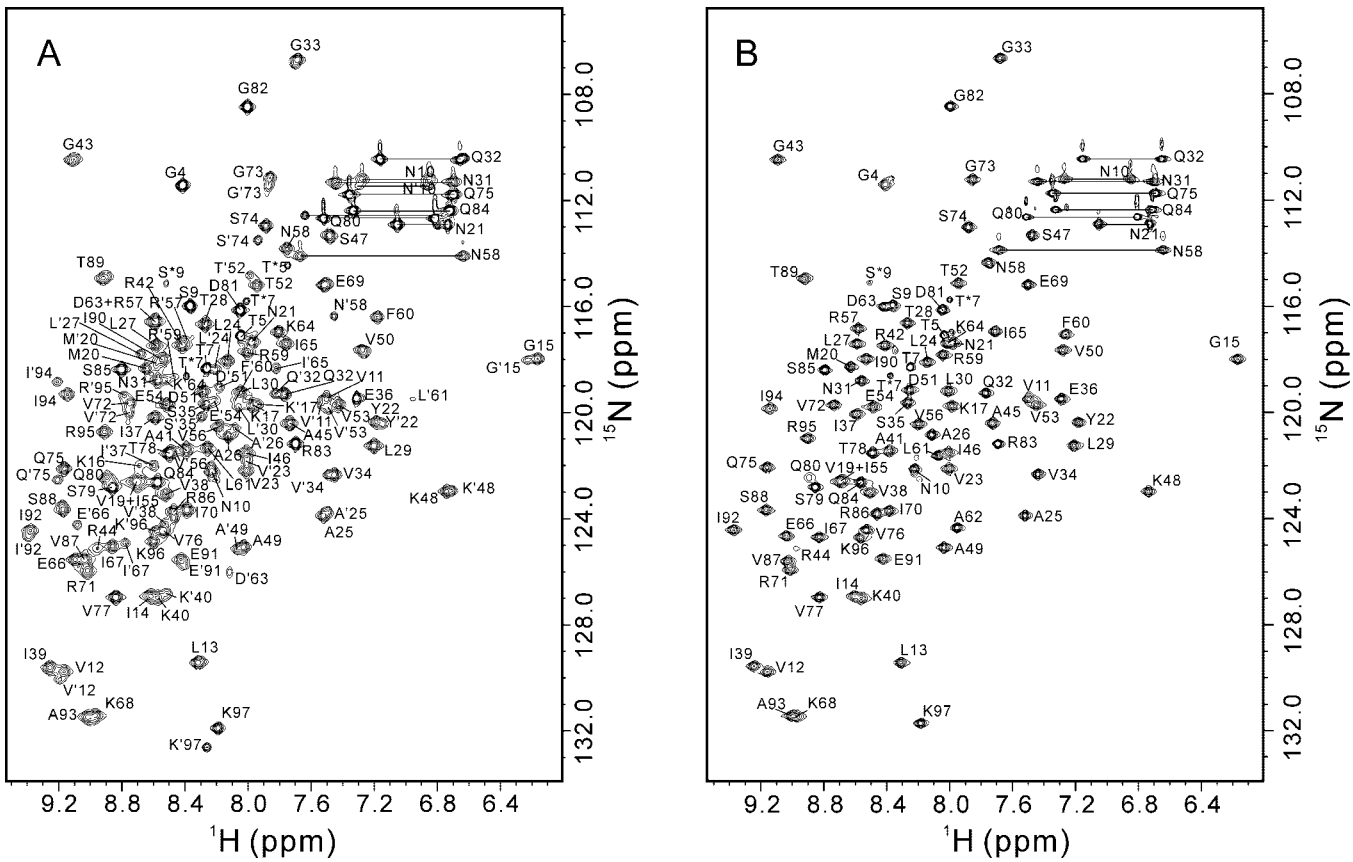

FIG. 1. **2D ^{1}H-^{15}N HSQC spectra recorded at 310 K for Ssh10b (*A*) and [P62A]Ssh10b (*B*).** Resonance assignments are indicated with a one-letter amino acid code and residue number. Side-chain NH_2 resonances of Asn and Gln are connected by *horizontal lines*. Labels marked with a *star* for the cross-peaks of residues Thr^{5}, Thr^{7}, and Ser^{9} indicate the minor conformations caused by Pro^{6} and/or Pro^{8} isomerization. In *A*, the amino acid codes *with and without a prime* indicate the cross-peaks for the C-form and T-form of Ssh10b with low and high intensities, respectively.

classified by the exchange features, were observed for Ssh10b. Residues Thr^{5}, Thr^{7}, and Ser^{9} gave exchange cross-peaks (Fig. 5*A*) when the exchange delays were set in the range of 0.1 to 1.6s. However, the remaining doublets shown in Fig. 1*A* did not give any exchange cross-peaks at the same exchange delays but gave a result like that shown in Fig. 5*B* for residue Lys^{97}. Thr^{5}-Pro^{6}-Thr^{7}-Pro^{8}-Ser^{9} is an unstructured N-terminal segment of Ssh10b as determined by the chemical shift index (8). The appearances of the exchange cross-peaks of Thr^{5}, Thr^{7}, and Ser^{9} are clearly because of the *cis-trans* isomerization of the X-prolyl bonds in this segment. Thr^{7} is between Pro^{6} and Pro^{8} and therefore showed two minor peaks in Fig. 1*A* and four exchange cross-peaks in Fig. 5*A*. The intensity ratios of the major auto-peaks to the minor ones were about 11:1 at 310 K, a value much higher than that for the remaining doublets in Fig. 1*A*. Therefore, the remaining doublets were not caused by the *cis-trans* isomerization of Thr^{5}-Pro^{6} or Thr^{7}-Pro^{8} peptide bonds. This was confirmed by the 2D ^{1}H-^{15}N HSQC spectrum of [Δ8]Ssh10b (spectrum not shown), in which all resonance doublets remained the same as those in Fig. 1*A*, except for the absence of the cross-peaks for residues Gly^{4}, Thr^{5}, Thr^{7}, Ser^{9}, Met^{10}, and Val^{11}, because the N-terminal eight residues are truncated in [Δ8]Ssh10b molecule.

Ssh10b contains four prolines at positions 6, 8, 18, and 62 in the sequence. The 2D ^{1}H-^{15}N HSQC spectrum of [Δ8P18A]Ssh10b was almost the same as that of [Δ8]Ssh10b except for the appearance of a new cross-peak for Ala^{18} (data not shown). Thus, replacement of the proline by alanine at position 18 did not influence the conformational heterogeneity of the Ssh10b dimer.

Pro^{62} is located in the loop linking helix α_2 and strand β_3 (8). The P62A mutant Ssh10b ([P62A]Ssh10b) was confirmed to be a dimer in solution by diffusion measurements using the BPP-LED pulse sequence (18, 19) designed for determining the molecule size (data not shown). The 2D ^{1}H-^{15}N HSQC spectrum of [P62A]Ssh10b is shown in Fig. 1*B*. Only a single set of cross-peaks was observed for all residues except the residues Gly^{4}, Thr^{5}, Thr^{7}, Ser^{9}, and Asn^{10} of [P62A]Ssh10b. Substitution of Pro^{62} by Ala^{62} eliminated the *cis-trans* isomerization, so that the mutant Ssh10b dimer was found in a single conformational state. Overlay of Fig. 1, *B* and *A* shows that the cross-peaks of [P62A]Ssh10b can be mapped to the cross-peaks of the T-form of Ssh10b. This indicates that the T-form of the Ssh10b homodimer adopts the same conformation as that of the [P62A]Ssh10b homodimer.

Fig. 6*A* shows ^{1}H-^{1}H slices at the $^{13}C_{\alpha}$ frequencies of Leu^{61} and Pro-^{62} extracted from the 3D NOESY-^{1}H,^{13}C-HMQC (*lower strip*) and the 3D HCCH-TOCSY (*upper strip*) spectra for the T-form Ssh10b dimer, whereas Fig. 6*B* shows those for the C-form Ssh10b dimer. Two inter-residue NOE cross-peaks between $^{1}H_{\alpha}$ of Leu^{61} and $^{1}H_{\delta1}$ and $^{1}H_{\delta2}$ of Pro^{62} could be observed in the 3D NOESY-HMQC strip for the T-form Ssh10b dimer (Fig. 6*A*). The appearance of these two NOEs characterizes the *trans* conformation of the Leu^{61}-Pro^{62} peptide bond in the T-form Ssh10b dimer. In the strips corresponding to the C-form Ssh10b dimer (Fig. 6*B*), only one NOE cross-peak between the $^{1}H_{\alpha}$ resonances of Leu^{61} and Pro^{62} was observed. This NOE thus provides conclusive evidence that the Leu^{61}-Pro^{62} peptide bond in the C-form homodimer of Ssh10b is in a *cis* conformation. The above experimental results show that the global conformational heterogeneity of Ssh10b is the result of the *cis-trans* transformation of the Leu^{61}-Pro^{62} peptide bond of

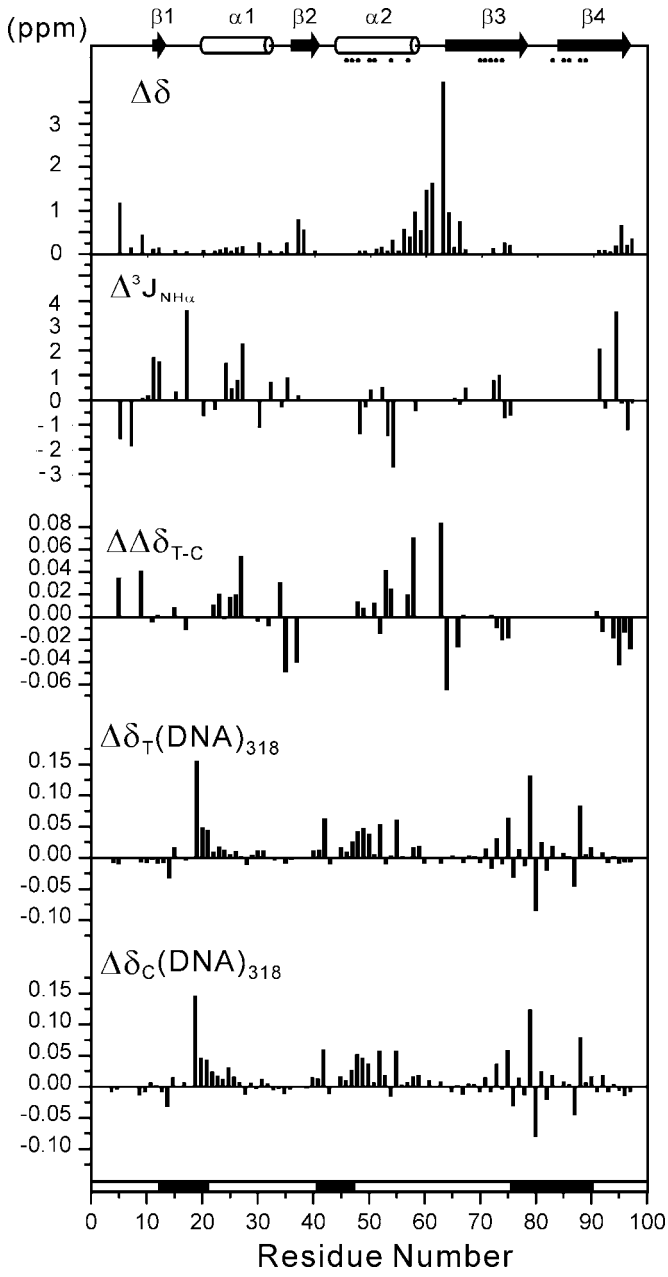

FIG. 2. **Differences of chemical shifts (Δδ) and J-coupling constants ($\Delta^3J_{NH\alpha}$) of the resonance doublets at 310 K and the changes in the ^1H_N chemical shifts *versus* residue number of Ssh10b.** Values of $\Delta\Delta\delta_{T\text{-}C}$ were obtained from experiments with the sample of Ssh10b at different temperatures. Values of $\Delta\delta_T(DNA)_{318}$ and $\Delta\delta_C(DNA)_{318}$ were obtained from the experiments with a sample of Ssh10b in complex with DNA at 318 K. Secondary structural elements of Ssh10b are labeled at the *top* of the figure. *Filled circles below* the secondary structural elements indicate the residues involved in the dimer interface. At the *bottom* of the figure, the *black bar* indicates the DNA binding regions.

the Ssh10b molecule. As expected given the predominately *trans* conformation of all amino acids other than proline, [P62A]Ssh10b appeared as a homodimer with the same conformation as that of the T-form homodimer of the Ssh10b molecule.

^1H_N Resonances for the T-form and C-form Ssh10b Dimer at Different Temperatures—To study the temperature-dependent features of Ssh10b, 2D ^1H-^{15}N HSQC spectra were recorded at different temperatures for a sample in 20 mM sodium acetate buffer, pH 5.0 containing 20 mM KCl (spectra not shown). The population ratios of the C-form to the T-form of Ssh10b were

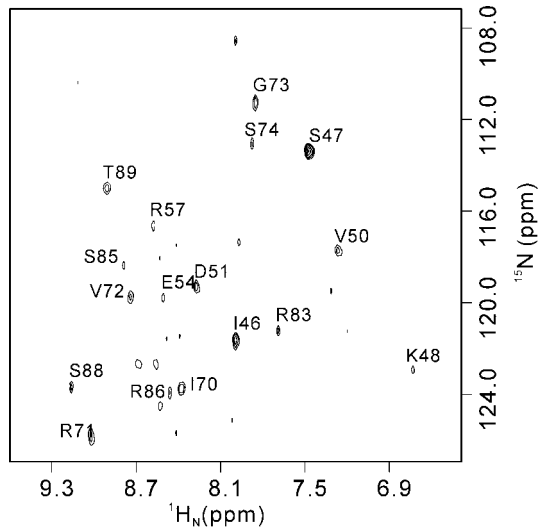

FIG. 3. **Residues involved in the dimer interface of Ssh10b.** The assigned cross-peaks are labeled with the one-letter amino acid code and residue number.

obtained by measuring the intensities of the corresponding cross-peaks for both conformations over the temperature range 283 to 330 K (Fig. 7). The ratio of C-form to T-form was around 0.26 at 318 K and greater than 0.6 below 298 K. Clearly, the T-form of the Ssh10b dimer is dominant, although the population of the C-form increases on decreasing the temperature.

The ^1H_N chemical shifts of all resolved cross-peaks in the 2D ^1H-^{15}N HSQC spectra were measured at different temperatures for the T-form and the C-form Ssh10b dimers. The differences between the ^1H_N chemical shifts at 298 K (δ_{298}) and at 318 K (δ_{318}) for the T-form ($\Delta\delta_T = \delta_{T298} - \delta_{T318}$) and the C-form ($\Delta\delta_C = \delta_{C298} - \delta_{C318}$) of a Ssh10b sample containing a high concentration of salt (200 mM KCl), and $\Delta\delta_T = \delta_{T300} - \delta_{T320}$ and $\Delta\delta_C = \delta_{C300} - \delta_{C320}$ of a Ssh10b sample containing a low concentration of salt (20 mM KCl), were obtained (data not shown). On increasing the temperature, the ^1H_N chemical shifts of the majority of the cross-peaks were shifted upfield ($+\Delta\delta$) for both the T-form and the C-form Ssh10b dimers. However, this was not the case for residues Ala^{25}, Leu^{48}, Val^{53}, Arg^{57}, and Leu^{61} of the C-form of Ssh10b in the sample containing 20 mM KCl and for residues Asn^{58} and Asp^{63} of the C-form of Ssh10b in the sample containing 200 mM KCl, which all showed downfield shifts ($-\Delta\delta$) on increasing the temperature.

The extent of upfield movements of the ^1H_N chemical shifts ($+\Delta\delta$) varied for the residues in the Ssh10b dimer that generated resonance doublets. The differences between the changes in the ^1H_N chemical shifts of the resonances for the T-form and for the C-form of Ssh10b ($\Delta\Delta\delta_{T\text{-}C} = \Delta\delta_T - \Delta\delta_C$), obtained from the data of the Ssh10b sample containing 200 mM KCl at temperature of 298 and 318 K, are shown in Fig. 2 and also mapped onto 3D structure (Fig. 4*C*). For residues Tyr^{22}, Val^{23}, Ala^{25}, Ala^{26}, and Leu^{27}, located in helix α_1, and residues Lys^{48}, Asp^{51}, Val^{53}, Glu^{54}, Arg^{57}, and Asn^{58}, located in helix α_2, the $\Delta\Delta\delta_{T\text{-}C}$ values are larger than +0.01 ppm. Residues Val^{34}, located in the turn between helix α_1 and strand β_2, and Asp^{63}, in the loop linking helix α_2 and strand β_3, also showed $+\Delta\Delta\delta_{T\text{-}C}$ (>0.01 ppm). However, negative $\Delta\Delta\delta_{T\text{-}C}$ with absolute values larger than 0.01 ppm were observed for residues Ser^{35} and Ile^{37} at the N terminus of strand β_2, residues Lys^{64}, Glu^{66}, Gly^{73}, Ser^{74}, and Gln^{75} in strand β_3, and residues Ile^{92}, Ile^{94}, Arg^{95}, Lys^{96}, and Lys^{97} at the C terminus of strand β_4 (Fig. 2). Thus, the upfield shifts of the ^1H_N resonances of the residues in helices α_1 and α_2 of the T-form were larger than those of the

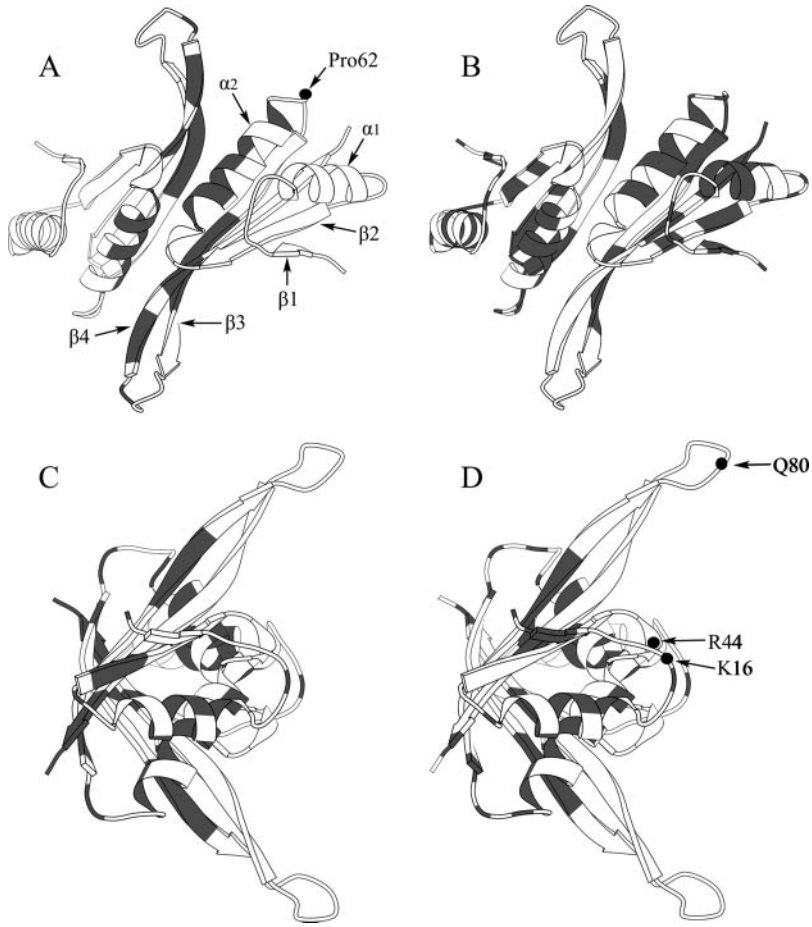

FIG. 4. **Ribbon diagram of monomeric unit of Alba structure (7).** Mapping of the residues on 3D Alba structure is shown. *Black* color indicates the residues at the dimer interface; *A*, the residues generating the resonance doublet; *B*, the residues showing the values of $\Delta\Delta\delta_{T\text{-}C} > 0.01$ ppm; *C*, the residues providing the differences in the chemical shift perturbations by DNA binding between two forms of DNA-Ssh10b complexes; *D*, the positions of secondary structure elements and residues Lys^{16}, Arg^{44}, Pro^{62}, and Gln^{80} are indicated.

C-form on increasing the temperature. However, for residues involved in formation of the β_2-β_4-β_3 antiparallel β-sheet, the upfield shifts of the ^1H_N resonances of the T-form were smaller than those of the C-form when the temperature was increased. This provides further evidence for conformational differences, in particular different strength of hydrogen bonding, in the two forms of the Ssh10b dimers.

NMR Spectral Features of the dsDNA-Ssh10b Complex at Different Temperatures—The 2D ^1H-^{15}N HSQC spectra of Ssh10b and the dsDNA-Ssh10b complex in sodium acetate buffer, pH 5.5, containing 200 mM KCl were recorded at temperatures of 318 and 298 K for a Ssh10b:DNA ratio of 1:3 (spectra not shown). The ^1H_N chemical shifts of all resolved cross-peaks in the 2D ^1H-^{15}N HSQC spectra of Ssh10b (δ) and of Ssh10b in complex with DNA (δ(DNA)) were measured. The differences of $\Delta\delta$(DNA) from δ of the cross-peaks ($\Delta\delta$(DNA) = δ(DNA) − δ) were obtained for both the T-form ($\Delta\delta_T$(DNA)) and the C-form ($\Delta\delta_C$(DNA)) Ssh10b molecules at 318 K ($\Delta\delta_T(DNA)_{318} = \delta_T(DNA)_{318} - \delta_{T318}$, $\Delta\delta_C(DNA)_{318} = \delta_C(DNA)_{318} - \delta_{C318}$) and at 298 K ($\Delta\delta_T(DNA)_{298} = \delta_T(DNA)_{298} - \delta_{T298}$, $\Delta\delta_C(DNA)_{298} = \delta_C(DNA)_{298} - \delta_{C298}$). The $\Delta\delta$(DNA) values represent the changes in the ^1H_N chemical shifts of Ssh10b on binding to dsDNA.

The histograms showing the chemical shift changes of the ^1H_N resonances for both the T-form and C-form Ssh10b dimers upon addition of dsDNA at a temperature of 318 K ($\Delta\delta_T(DNA)_{318}$ and $\Delta\delta_C(DNA)_{318}$) are shown in Fig. 2. $\Delta\delta_T(DNA)_{318}$ and $\Delta\delta_C(DNA)_{318}$ with absolute values larger than 0.02 ppm appear in three regions of the Ssh10b molecule. The first region includes helix α_1 and the loop linking strand β_1 and helix α_1, the second one is the C-terminal of strand β_2 and helix α_2, and the third one consists of the C terminus and the N terminus of strands β_3 and β_4, respectively, and the β-turn between them (Fig. 2). $\Delta\delta_T(DNA)_{298}$, and $\Delta\delta_C(DNA)_{298}$ (data not shown) showed similar histograms to that of $\Delta\delta_T(DNA)_{318}$ and $\Delta\delta_C(DNA)_{318}$. $\Delta\delta$(DNA) values provided information about the location of DNA binding sites and the local conformational changes of the Ssh10b dimer induced by binding of DNA.

Compare the values of $\Delta\delta_T(DNA)_{318}$ and $\Delta\delta_T(DNA)_{298}$ with $\Delta\delta_C(DNA)_{318}$ and $\Delta\delta_C(DNA)_{298}$, respectively, and the differences in the ^1H_N chemical shift perturbations by DNA binding between two forms of Ssh10b dimer can be noticed. The residues showing the observable differences are indicated in the 3D structure (Fig. 4*D*). The differences were found mainly in two helices and in three β strands. However, upon interaction with DNA, ^1H_N resonances of the residues in the segments, Ala^{41}-Ser^{47} and Val^{76}-Ile^{90}, still remain as singlet. It seems that DNA binding produces similar conformational changes to these two polypeptide segments in the two forms of the Ssh10b molecule, although different changes in the ^1H_N resonances between the two forms of the Ssh10b dimer are observed in other regions of the polypeptide chain of the molecule.

Temperature-dependent Interaction of DNA with Ssh10b and [P62A]Ssh10b—The interaction of DNA with the Ssh10b dimer has been found to be temperature-dependent (1). To further investigate the temperature-dependent features of DNA binding, EMSA and nick closure assays were performed on both Ssh10b and the P62A-mutant Ssh10b ([P62A]Ssh10b) under identical experimental conditions.

In the EMSA assay, a ^{32}P-labeled 108-bp dsDNA fragment (0.5–1 ng) was mixed with different amounts of Ssh10b or [P62A]Ssh10b and analyzed by gel electrophoresis at 293 and 320 K. The bands show the distribution of the products of the DNA-protein interaction by complex size (Fig. 8). The apparent K_d was

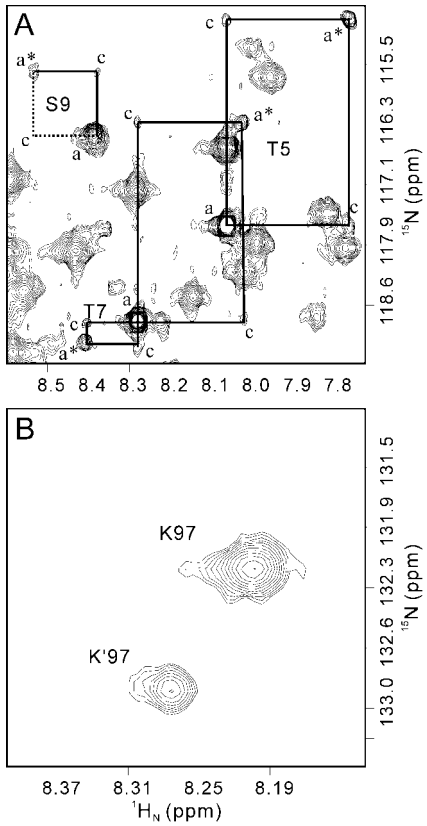

FIG. 5. **Portions of the heteronuclear chemical exchange spectrum at an exchange delay of 1.3 s.** *A*, spectral region showing the chemical exchange cross-peaks between the resonance doublets of residues Thr[5], Thr[7], and Ser[9] (*a*, auto peak; *c*, exchange cross-peak). Three auto peaks exist for Thr[7] and are still called a doublet indiscriminately for simplicity in the text. The *star* on the *letter a* indicates minor resonances of the doublets. *B*, cross-peaks of residue Lys[97]. No chemical exchange happens between the remaining resonance doublets at the experimental delay time, as exemplified by Lys[97].

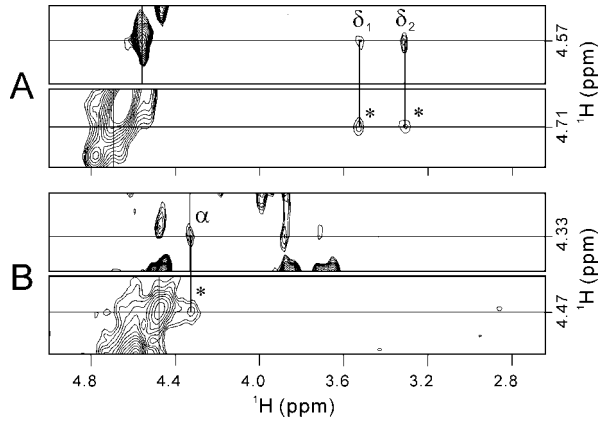

FIG. 6. **Strip plots of 2D ^{1}H-^{1}H planes from the 3D NOESY-^{1}H, ^{13}C-HMQC, and HCCH-TOCSY spectra of ^{13}C-labeled Ssh10b in the T-form (*A*) and C-form (*B*).** In both *A* and *B*, the *upper strips* are from the 3D HCCH-TOCSY spectrum, and the *lower strips* are from the 3D NOESY-HMQC spectrum. Strips of 3D NOESY-HMQC and HCCH-TOCSY spectra are extracted at $^{13}C_\alpha$ frequencies of Leu[61] (*A*, 53.32 ppm; *B*, 54.68 ppm) and Pro[62] (*A*, 64.59 ppm; *B*, 63.66 ppm), respectively. The *star* indicates the NOE cross-peaks.

about 0.04 μM estimated by the amount of protein required to retard 50% of the DNA. The cooperative binding of Ssh10b to DNA was observed; therefore the ratio of protein:DNA influenced the migration pattern of the DNA-protein complexes in EMSA. The DNA-Ssh10b and DNA-[P62A]Ssh10b complexes showed similar migration patterns at 293 and 320 K when the concentration of the protein was lower, such as 0.04 μM (*lane 1* in Fig. 8) or 0.08 μM (*lane 2* in Fig. 8). However, when the protein concentration was higher, such as 0.16 or 0.32 μM, the nature of cooperative binding of Ssh10b to DNA makes the migration patterns of the DNA-Ssh10b complexes at 320 K totally different from those at 293 K, but resemble those of the DNA-[P62A]Ssh10b complexes at both temperatures (*lanes 3* and *4* in Fig. 8). Therefore, the mode of binding of the Ssh10b dimer to DNA in the complex at 293 K must be different from that at 320 K or in the DNA-[P62A]Ssh10b complex at either temperature.

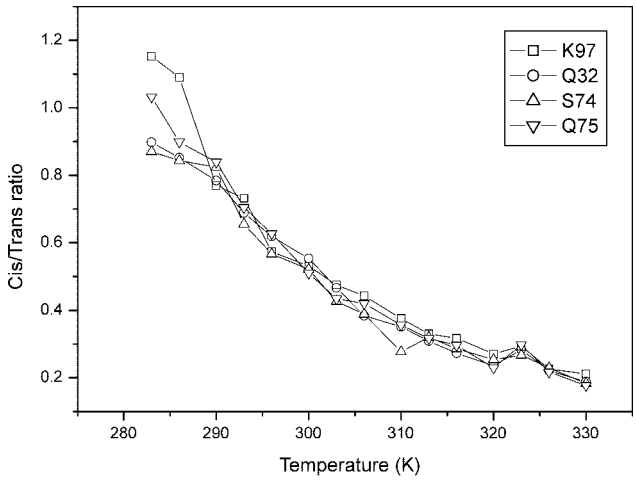

FIG. 7. **Population ratio of C-form/T-form Ssh10b homodimer *versus* temperature for residues Gln[32], Ser[74], Gln[75], and Lys[97].** Populations are measured as the intensities of the cross-peaks.

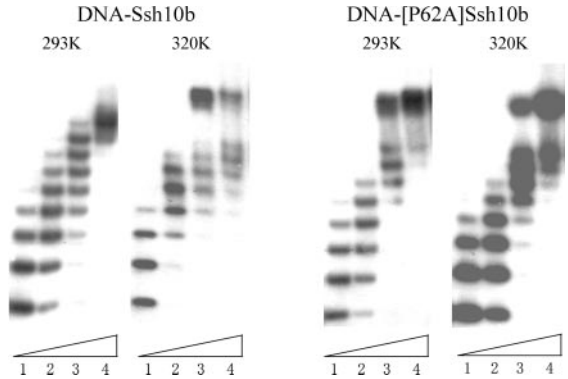

FIG. 8. **EMSA bands of DNA-Ssh10b and DNA-[P62A]Ssh10b complexes at temperatures of 293 and 320 K.** The concentration of proteins is 0.04 μM (*lane 1*), 0.08 μM (*lane 2*), 0.16 μM (*lane 3*), and 0.32 μM (*lane 4*). The gel of Ssh10b at 320 K was slightly under-exposed to x-ray film, and that of [P62A]Ssh10b at 320 K was over-exposed.

Nick closure assays were carried out to detect the capabilities of the proteins to constrain DNA in supercoils at 298 or 330 K. In the nick closure assay, a single-nick plasmid pUC18 was ligated in the absence and presence of the proteins. The results for different protein:DNA ratios is shown in Fig. 9. The assay in the absence of protein (*lane 1* in Fig. 9) was performed as a control. At 298 K, addition of Ssh10b to the reaction mixture produced only a weak CCC (covalently closed circular plasmid) band with a high supercoil density at a protein:DNA mass ratio of 2:1 (Fig. 9, *upper left panel*, *lane 4*). However, at 330 K the ability of the bound Ssh10b to introduce supercoils into the plasmid increases dramatically. [P62A]Ssh10b showed similar ability to introduce supercoils into the plasmid at 330 K. However, unlike bound Ssh10b at 298 K, [P62A]Ssh10b was capable of introducing supercoils into the plasmid over the whole range of the protein concentrations at 298 K (Fig. 9, *lower left panel*). Clearly, the abilities of Sshb10b and [P62A]Ssh10b to affect the

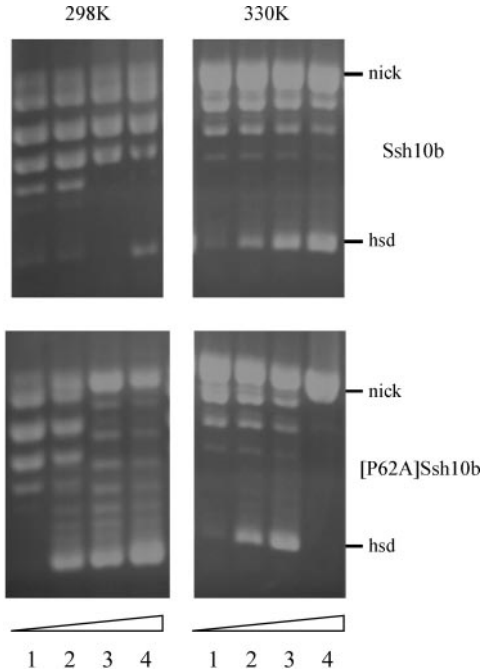

FIG. 9. **Nick closure assays of Ssh10b and [P62A]Ssh10b at temperatures of 298 and 330 K.** The protein/DNA mass ratio is 0:1 (*lane 1*), 0.5:1 (*lane 2*), 1:1 (*lane 3*), and 2:1 (*lane 4*). *Nick* denotes nicked plasmids, and *hsd* denotes the CCC (covalently closed circular plasmid) band with a high supercoil density. The abnormal disappearance of the hsd band in *lane 4* of [P62A]Ssh10b at 330 K is because of the blockage of the sites in the DNA for ligase by too much bound [P62A]Ssh10b.

topology of DNA are similar at high temperature (330 K) but different at low temperature (298 K).

The results of EMSA and nick closure assays indicate that [P62A]Ssh10b, existing in a single *trans* conformation in solution, shows the same features upon interaction with DNA at both high and low temperatures. Therefore, the temperature-dependent nature of the interaction of Ssh10b with DNA correlates with the two conformations of the Ssh10b dimer.

DISCUSSION

Different Conformational Features of the T-form and C-form Ssh10b Homodimer—The conformational features of a protein are strongly influenced by factors that affect the strength of intramolecular hydrogen bonds. Changes in the chemical shifts of ^1H_N resonance are a sensitive indicator of changes in the strength of hydrogen bonding. The chemical shifts of ^1H_N resonances are affected by hydrogen bond acceptors, particularly carbonyl groups (20, 21). Wagner and co-workers (22, 23) demonstrated that ^1H_N chemical shifts depend on the inverse third power of the distance between the ^1H_N and the hydrogen bond acceptor. In the case of hydrogen bonding with C=O, large downfield shifts are observed for strongly hydrogen-bonded amide protons. Within protein secondary structure, the ^1H_N of the *i*th residue forms a hydrogen bond with the C=O of the (*i*-4)th residue in an α-helix, and in an antiparallel β-sheet, the ^1H_N and the C=O of a residue in one β strand forms hydrogen bonds with the C=O and the ^1H_N of a residue in the opposite strand. When the temperature is increased, the thermal fluctuations of an α-helix or a β-sheet are enlarged, and the average distance between the ^1H_N and the C=O increases. As a consequence of weakened hydrogen bonding, the chemical shifts of the ^1H_N resonances will tend to move upfield.

The ^1H_N resonances of almost all cross-peaks in the 2D ^1H-^{15}N HSQC spectrum of the Ssh10b molecule were shifted upfield on increasing the temperature. This is thus consistent with a general weakening of the hydrogen bonding in both the T-form and the C-form of the Ssh10b dimer on increasing the temperature. However, the temperature-dependent shifts of the ^1H_N resonances were different in size for the T-form ($\Delta\delta_T$) and the C-form ($\Delta\delta_C$). This then suggests a difference between the hydrogen bonding strengths within the secondary structure of the two forms of the Ssh10b dimer. The values of $\Delta\Delta\delta_{T\text{-}C} = \Delta\delta_T - \Delta\delta_C$ for each residue are shown in Fig. 2. On increasing the temperature, the residues in helices α_1 and α_2 show larger upfield shifts of the ^1H_N resonances for the T-form ($+\Delta\Delta\delta_{T\text{-}C}$), whereas the residues involved in the antiparallel β-sheet show larger upfield shifts for the C-form ($-\Delta\Delta\delta_{T\text{-}C}$) (Fig. 2). In the antiparallel β-sheet formed by β_2-β_4-β_3 strands, the ^1H_N and C=O groups of residues Ile^{94}, Arg^{95}, Lys^{96}, and Lys^{97} form hydrogen bonds with C=O and ^1H_N of Ile^{37}, Glu^{66}, Ser^{35}, and Lys^{64}, respectively. Residues Ile^{94}, Arg^{95}, Lys^{96}, and Lys^{97} are located in the C-terminal of strand β_4. Residues Ile^{37} and Ser^{35} are located in the N-terminal region of strand β_2, and Glu^{66} and Lys^{64} are located in the N-terminal region of strand β_3. Thus, on increasing the temperature, the lengthening of the hydrogen bond distances in the portion of antiparallel β-sheet near to the C-terminal of the Ssh10b molecule is greater for the C-form than that for the T-form Ssh10b dimer. Conversely, the lengthening of the hydrogen bond distances in the α-helices is greater for the T-form. These results suggest that the spatial packing of the residues is tighter in the α-helices and looser in the portion of the antiparallel β-sheet near the C-terminal of the molecule for the C-form than that for the T-form of Ssh10b molecule.

Further support for different temperature-dependent features of the secondary structure of the T-form and the C-form of the Ssh10b dimer was from the observation that for a few ^1H_N resonances, the direction of the temperature-dependent shift is different in the two forms. The ^1H_N resonances of residues Ala^{25}, Leu^{48}, Val^{53}, Arg^{57}, and Leu^{61} for the sample containing 20 mM KCl, and of residues Asn^{58} and Asp^{63} for the sample containing 200 mM KCl, shifted downfield for the C-form and upfield for the T-form of Ssh10b molecule. Residues Ala^{25}, Leu^{48}, Val^{53}, Arg^{57}, and Asn^{58} are located in α-helices. Leu^{61} and Asp^{63} are the nearest neighbors of Pro^{62}, located in the loop linking helix α_2 and strand β_3. The magnitudes of downfield shifts of the ^1H_N resonances of these residues upon increasing temperature were in the range 0.6~2.8 ppb/K. In addition, the $\Delta^3J_{NH\alpha}$ values for residues Leu^{24}, Leu^{27}, Lys^{48}, Val^{53}, and Glu^{54} were all greater than $\pm$1 Hz (Fig. 2), corresponding to a change in backbone torsion angle, $\Delta\phi > \pm 10°$, between the two forms of Ssh10b molecule. Residues Ala^{25} and Asn^{58} also showed small variations of $\Delta^3J_{NH\alpha}$ (Fig. 2). Thus, differences in the hydrogen bonding strengths in the secondary structure of the two forms correlate with main-chain conformational differences between the T-form and the C-form Ssh10b molecule.

DNA Binding Sites on the T-form and the C-form ssh10b Dimers—Proteins bind in the major or minor grooves of DNA and some protein structures have contacts with DNA in both grooves simultaneously (24). In the model proposed for the DNA-Alba complex (7), the Alba dimer interacts simultaneously with a major groove and the two flanking minor grooves of the DNA. Residues Lys^{16}, Lys^{17}, and Arg^{42} in the central "belly" of Alba dimer are involved in DNA binding at the major groove, and the β-hairpin of Alba interacts with the minor grooves.

Ssh10b lacks the first three N-terminal amino acid residues of Sso10b but is otherwise identical in sequence. In fact, the protein used to solve Alba crystal structure is identical with Ssh10b (7). Thus, Ssh10b is supposed to have the same DNA binding sites shown by the DNA-Alba complex. Examination of the interaction of the Ssh10b dimer with DNA in solution by NMR spectroscopy revealed the location of the DNA binding sites on both the T-form and the C-form Ssh10b molecule. The DNA binding regions of the

T-form and C-form Ssh10b dimers at 318 K are apparent from the DNA-induced changes in chemical shift values, $\Delta\delta_T(DNA)_{318}$ and $\Delta\delta_C(DNA)_{318}$ (Fig. 2). Three regions of the Ssh10b molecule can be identified as involved in DNA binding: Val^{76}-Ile^{90}, a region spanning the C-terminal of strand β_3, the N-terminal of strand β_4, and the β-turn between them. Inspection of the amino acid sequence of the Ssh10b molecule indicates that a group of polar residues, Ser^{74}, Gln^{75}, Thr^{78}, Ser^{79}, Gln^{80}, Gln^{84}, Ser^{85}, Ser^{88}, and Thr^{89}, is clustered in this region. The β-turn also contains a positively charged residue, Arg^{83}. Positively charged and polar residues complement the negative charges on the DNA (24). Therefore, it is reasonable to conclude that the β-turn region of the Ssh10b dimer binds in the minor grooves of dsDNA as suggested by the DNA-Alba dimer complex (7). The other two regions, Leu^{13}-Asn^{21} and Ala^{41}-Ser^{47}, include the loop linking strand β_1 and helix α_1 and a segment spanning the C-terminal of strand β_2 and the N-terminal of helix α_2. The former contains Lys^{16} and Lys^{17}, and the latter contains Lys^{40}, Arg^{42}, and Arg^{44}, which form a cluster of positively charged residues in the Ssh10b molecule. This cluster is around 22 Å distant from the β-turn in the DNA-Alba dimer complex, and a similar distance was observed in the DNA-Ssh10b dimer complex.[2] This therefore implies that this cluster of positively charged residues in the Ssh10b dimer can make contact with the major groove of the DNA.

The T-form and C-form Ssh10b dimers appear to have the same binding sites for DNA at both 298 and 318 K, deduced from the fact that $\Delta\delta_T(DNA)_{298}$ and $\Delta\delta_C(DNA)_{298}$ show similar histograms to that of $\Delta\delta_T(DNA)_{318}$ and $\Delta\delta_C(DNA)_{318}$ (Fig. 2). In addition, very weak signals were observed for residues Lys^{16}, Arg^{44}, and Gln^{80} (see Fig. 1 and Fig. 4*D*), which become stronger when DNA is bound. This provides further verification of the regions of the Ssh10b dimer involved in DNA binding.

Origin of the Temperature-dependent Interactions of dsDNA with the Ssh10b Dimer—On the basis of the different relative populations of the T-form and the C-form of the Ssh10b dimer at different temperatures (Fig. 7), the temperature-dependent features of the interaction of DNA with the Ssh10b dimer revealed by the EMSA (Fig. 8, *left two panels*) and nick closure (Fig. 9, *upper two panels*) assays are presumably related to the different conformational features of the T-form and C-form of the Ssh10b dimer and to the different conformational changes of these two forms while interacting with DNA.

When protein binds to DNA, conformational changes occur in both the protein and the DNA (24, 25). As can be seen in Fig. 2, $\Delta\delta_T(DNA)_{318}$, $\Delta\delta_T(DNA)_{298}$, $\Delta\delta_C(DNA)_{318}$, and $\Delta\delta_C(DNA)_{298}$ showed values larger than ± 0.02 ppm for residues in the α-helix and β-sheet that were not in contact with DNA. This is presumably because of conformational changes induced by the binding of DNA. Because the residue packing in the two forms of the Ssh10b molecule is different, this could then lead to different conformational changes on binding of DNA. Such differences between the T-form and the C-form are mainly observed in regions not involved in DNA-Ssh10b interfaces (Fig. 4*C*). For DNA binding regions, residues Ala^{41}-Ser^{47} and Val^{76}-Ile^{90}, show similar changes in the main-chain conformations of the segments in the DNA-T-form and the DNA-C-form. The chemical shifts of the ^1H_N resonances for Gly^{15} and Lys^{17} in the segment Leu^{13}-Asn^{21} are also relatively small (Fig. 2). Therefore, the T-form and the C-form of the Ssh10b molecule can be considered to have similar main-chain conformational features for the DNA binding regions in the DNA-Ssh10b dimer complex. This implies that the mode of contact with DNA in the two forms of the Ssh10b dimer is the same. Many studies have reported that DNA structure can be forcibly distorted by the binding of proteins (17, 24, 26, 27). For some protein-DNA complexes, the dimensions of the DNA grooves are adjusted to the correct separation to allow the binding of protein elements. It is therefore possible that the conformations of DNA may change when the T-form or the C-form Ssh10b dimer is bound.

Concerning the mode of interaction of the T-form and the C-form of the Ssh10b dimer with DNA, the above analysis allows the following model to be proposed: the relative spatial positions of the β-turn and the belly of the Ssh10b dimer in the C-form may deviate from that in the T-form Ssh10b molecule. This deviation may increase when DNA interacts with the Ssh10b dimer. Because the DNA-Ssh10b dimer interfaces remain the same for the T-form and the C-form and have similar main-chain conformational features, the DNA may have to undergo some adjustment in conformation to facilitate binding with the two forms of the Ssh10b dimer. Consequently, the conformations of DNA and the Ssh10b dimer in the DNA-T-form complex may help to constrain DNA in supercoils but not in the DNA-C-form complex. The results of EMSA and nick closure assays with [P62A]Ssh10b (see Fig. 8, *right two panels* and Fig. 9, *lower two panels*) show that the T-form, which is favored at high temperature, is the form of Ssh10b that causes DNA to adopt a supercoiled formation. This then provides direct evidence that the co-existence of two forms of the Ssh10b dimer is the origin of the temperature-dependent interaction of the Ssh10b dimer with DNA.

Acknowledgment—We thank Professor Sarah Perrett for critically reading the manuscript.

[2] Q. Cui, Y. Tong, and J. Wang, unpublished data.

REFERENCES

1. Xue, H., Guo, R., Wen, Y., Liu, D., and Huang, L. (2000) *J. Bacteriol.* **182,** 3929–3933
2. Bell, S. D., Botting, C. H., Wardleworth, B. N., Jackson, S. P., and White, M. F. (2002) *Science* **296,** 148–151
3. Forterre, P., Confalonieri, F., and Knapp, S. (1999) *Mol. Microbiol.* **32,** 669–670
4. Dijk, J., and Reinhardt, R. (1986) in *Bacterial Chromatin* (Gualerzi, C. O., and Pon, C. L., eds) Springer-Verlag, New York
5. Grote, M., Dijk, J., and Reinhardt, R. (1986) *Biochim. Biophys. Acta* **873,** 405–413
6. Lurz, R., Grote, M., Dijk, J., Reinhardt, R., and Dobrinski, B. (1986) *EMBO J.* **5,** 3715–3721
7. Wardleworth, B. N., Russell, R. J., Bell, S. D., Taylor, G. L., and White, M. F. (2002) *EMBO J.* **21,** 4654–4662
8. Tong, Y., Cui, Q., Feng, Y., Huang, L., and Wang, J. (2002) *J. Biomol. NMR* **22,** 385–386
9. Markley, J. L., Bax, A., Arata, Y., Hilbers, C. W., Kaptein, R., Sykes, B. D., Wright, P. E., and Wuthrich, K. (1998) *J. Biomol. NMR* **12,** 1–23
10. Farrow, N. A., Zhang, O., Forman-Kay, J. D., and Kay, L. E. (1994) *J. Biomol. NMR* **4,** 727–734
11. Muhandiram, D. R., Xu, G. Y., and Kay, L. E. (1993) *J. Biomol. NMR* **3,** 463–470
12. Permi, P., Kilpelainen, I., Annila, A., and Heikkinen, S. (2000) *J. Biomol. NMR* **16,** 29–37
13. Sambrook, J., Fritsch, E. F., and Maniatis, T. (1989) *Molecular Cloning: A Laboratory Manual*. 2nd Ed., Vol. 3, p. B.23, Cold Spring Harbor Laboratory Press, Cold Spring Harbor, New York
14. Clark, D. J., and Felsenfeld, G. (1991) *EMBO J.* **10,** 387–395
15. Mai, V. Q., Chen, X., Hong, R., and Huang, L. (1998) *J. Bacteriol.* **180,** 2560–2563
16. Ogura, K., Nagata, K., Horiuchi, M., Ebisui, E., Hasuda, T., Yuzawa, S., Nishida, M., Hatanaka, H., and Inagaki, F. (2002) *J. Biomol. NMR* **22,** 37–46
17. Olson, W. K., Gorin, A. A., Lu, X. J., Hock, L. M., and Zhurkin, V. B. (1998) *Proc. Natl. Acad. Sci. U. S. A.* **95,** 11163–11168
18. Jones, J. A., Wilkins, D. K., Smith, L. J., and Dobson, C. M. (1997) *J. Biomol. NMR* **10,** 199–203
19. Wilkins, D. K., Grimshaw, S. B., Receveur, V., Dobson, C. M., Jones, J. A., and Smith, L. J. (1999) *Biochemistry* **38,** 16424–16431
20. Baxter, N. J., and Williamson, M. P. (1997) *J. Biomol. NMR* **9,** 359–369
21. Cierpicki, T., and Otlewski, J. (2001) *J. Biomol. NMR* **21,** 249–261
22. Pardi, A., Wagner, G., and Wuthrich, K. (1983) *Eur. J. Biochem.* **137,** 445–454
23. Wagner, G., Pardi, A., and Wuthrich, K. (1983) *J. Am. Chem. Soc.* **105,** 5948–5949
24. Jones, S., van Heyningen, P., Berman, H. M., and Thornton, J. M. (1999) *J. Mol. Biol.* **287,** 877–896
25. Pabo, C. O., and Sauer, R. T. (1992) *Annu. Rev. Biochem.* **61,** 1053–1095
26. Schultz, S. C., Shields, G. C., and Steitz, T. A. (1991) *Science* **253,** 1001–1007
27. Winkler, F. K., Banner, D. W., Oefner, C., Tsernoglou, D., Brown, R. S., Heathman, S. P., Bryan, R. K., Martin, P. D., Petratos, K., and Wilson, K. S. (1993) *EMBO J.* **12,** 1781–1795